Engineering Geology 195 (2015) 111–121

Contents lists available at ScienceDirect

Engineering Geology

journal homepage: www.elsevier.com/locate/enggeo

Monitoring landslide displacements with the Geocube wireless network of low-cost GPS

L. Benoit [a,*], P. Briole [b], O. Martin [a], C. Thom [a], J.-P. Malet [c], P. Ulrich [c]

[a] IGN, DRE/SRIG/LOEMI, 73 avenue de Paris, 94160 Saint-Mandé, France
[b] ENS, Laboratoire de Géologie, CNRS UMR 8538, 24 Rue Lhomond, 75231 Paris Cedex 5, France
[c] Institut de Physique du Globe de Strasbourg, CNRS UMR 7516, EOST/Université de Strasbourg, 5 rue Descartes, 67084 Strasbourg Cedex, France

ARTICLE INFO

Article history:
Received 16 October 2014
Received in revised form 11 May 2015
Accepted 22 May 2015
Available online 6 June 2015

Keywords:
Landslide
Wireless sensor network
Low-cost GPS device
Dense GPS network

ABSTRACT

The analysis of landslide hazard requires continuous and high frequency surface displacement monitoring at numerous and geomorphologically relevant locations. Ground-based geodetic methods (GNSS, tacheometry) allow very accurate and high frequency temporal observations while remote sensing methods (InSAR, terrestrial and satellite photogrammetry, LIDAR) allow spatially distributed observations at high spatial resolution. A single surface deformation monitoring technique coupling all these capabilities is still missing.

The Geocube system has been designed to partly overcome this pitfall by creating a low-cost, flexible, easy to install and wireless GPS receiver. Dense Geocube monitoring networks can be set easily for operational observations. Furthermore, the monitoring of other landslide properties (micro-seismicity, seismic waves) or triggering factors (meteorology, slope hydrology) is possible with the capacity of integrating additional sensors to the Geocube.

This work presents the Geocube system and the results of a field campaign performed during the summer 2012 at the Super-Sauze landslide, southern French Alps, with a network of wireless low-cost GPS. The objective was to assess the performance of the Geocube system in real field monitoring conditions. Our results document the spatial and temporal evolution of the landslide during a period of 40 days. Landslide acceleration periods are detected and correlated to rainfall events.

1. Introduction

Detecting and identifying possible precursors of rapid landslide events (initial failure slope, acceleration of the moving masses, fluidization) requires high frequency monitoring and very high precision of the displacements measurements (Malet et al., 2002). A large variety of techniques is available for the monitoring of landslide displacements, ranging from classical ground-based geodetic methods (tachometry, Global Navigation Satellite System — GNSS — Malet et al., 2000, 2002), to remote sensing passive and active methods (optical, radar and LiDAR — Jaboyedoff et al., 2012). For surface displacement monitoring, ground based methods yield 3D measurements, a very high accuracy (typically in the range of a few millimeters) and high frequency observations (minutes to hours). However, these methods provide only a local (e.g., point) measurement of the deformation and thus a low spatial resolution. At the opposite, remote sensing methods provide dense displacement fields, but are characterized by low temporal resolution, and low accuracy (typically in the range of a few centimeters to decimeter, except for InSAR possibly attaining a few millimeters accuracy for the Up component). In addition these methods rarely provide 3D measurements, except for LiDAR observations (Travelletti et al., 2014). In this context, GNSS observations from geodetic dual-frequency receivers can be considered as a reference technique because of the possibility of high accuracy on the determination of the 3D locations at high temporal resolution (minutes to hours) and for all weather conditions. Moreover, GNSS monitoring systems are relatively easy to maintain and automate. However dual-frequency GNSS receivers are still expensive (in the range 5000 to 10,000 USD) which drastically limits either the number of monitoring points, or the region of interest to monitor to avoid possible loss of equipment.

In order to allow the deployment of dense GNSS networks on landslides, the unit price of each receiver has to be lowered. The use of less expensive single-frequency GNSS receivers is possible in case of landslides monitoring because their small size (a few hundreds of meters to 1 or 2 km) allows a relative positioning with short baselines (typically less than 5 km) which mitigates spatially correlated errors (such as ionospheric disturbances) and makes the use of L2 frequency unnecessary. Single-frequency receivers have been successfully used in the past for different landslide surveying tasks (Malet et al., 2000, 2002; Squarzoni et al., 2005; Heunecke et al., 2011).

In addition, during the last few years, single-frequency Global Positioning System (GPS) chips (up to now, only GPS is available, but chips with more GNSS constellations are scheduled in the coming

* Corresponding author at: IGN, LOEMI, 73 avenue de Paris, 94160 Saint-Mandé, France.
E-mail address: benoitlionel2@gmail.com (L. Benoit).

http://dx.doi.org/10.1016/j.enggeo.2015.05.020
0013-7952/

years) able to record raw carrier phase data at a low energy consumption rate are available on the market for around 100 USD. These chips acquire L1 frequency data in the same way as geodetic receivers. In order to obtain low-cost monitoring devices, the GPS antennas are small and basic, and this simplicity leads to a lower multipath rejection than larger and more expensive geodetic GNSS antennas (e.g., choke-ring) leading to a slightly degraded accuracy. Such GPS chip and antenna can be used to design low-cost, compact and flexible GPS receivers using low-power (10 W) solar panels that can be easily installed in the field for continuous data acquisition. Integrating a radio link to the receivers allows wireless and real-time data exchange. Distant receiver settings and real-time positioning are then possible (Cattin and Brahier, 2011).

The miniaturization of the electronic components impacts also the environmental sensors allowing the monitoring of, for instance, the soil/air temperature, the soil water content and the pore water fluid pressure. Using for example MEMS (Micro-Electro-Mechanical Systems) sensors, the receivers can acquire other observations in complement to positioning observations. Such device corresponds to the concept of geo-localized multi-sensors (Azzam et al., 2010; Peters et al., 2010; Buchli et al., 2012). The Geocube system has been developed by the French National Institute of Geographic and Forest Information (IGN — Institut National de l'Information Géographique et Forestière) to combine these two concepts of wireless network of low-cost GPS and multi-sensor receiver.

In this work, we present the Geocube system and benchmark its performance and accuracy in real field monitoring conditions at an active landslide. First, the technology of the Geocube system, the characteristics of the network operation mode and the principles of the calculation of the positions are presented. The capability of the positioning algorithm to measure several types of movement expected in the case of landslide monitoring is discussed. Second, the characteristics of the field acquisition carried out at the highly documented Super-Sauze landslide are presented. This landslide is monitored by the French Landslide Observatory (INSU-OMIV; http://omiv.unistra.fr). The hardware performances and the displacement measurements are assessed. Finally we discuss the contribution of Geocubes to detect transient acceleration/deceleration of the Super-Sauze landslide in summer 2012. During this period five rain events led to 130 mm cumulative rainfall, with a pick intensity reaching 30 $mm \cdot day^{-1}$. Simultaneously, the groundwater table in the landslide ranged between 1.40 m and 1.65 m below the topographic surface.

2. Characteristics of the Geocube system: instrument, network operation and data processing strategy

2.1. Technological design

Small low-cost GPS chips with low-power consumption are available on the market. Providing raw carrier phase observations, these instruments allow precise positioning (Takasu and Yasuda, 2008) and event dating. Similarly, an increased number of various small size environmental sensors are becoming available at low-cost. The coupling of GPS chips and other sensors to create geo-localized multi-sensors is of great interest. However data acquisition and management of all these sensors is still complex, mainly because of the necessity to combine several hardware interfaces.

The Geocube system was designed to overcome some of these limitations and has the following specifications:

1) The ability for sub-centimeter relative positioning within a local receiver network (<5 km extension);
2) The ability for precise measurement dating (10^{-4} s in standard operation mode) and synchronization in a single time scale of all sensors of all receivers in the network;
3) The ability for an easy integration of various sensor types offering a modular and flexible architecture;
4) The establishment of a wireless link for data exchange between the Geocube nodes;
5) The possibility to use small (30 cm × 35 cm, 10 W) solar panels for power supply;
6) The use of low-cost material to allow the setup of dense networks.

In order to implement these specifications, the Geocube is designed in three modules consisting of three electronic boards (Fig. 1):

- A GPS module (GPS board; Fig. 1) including a single-frequency *LEA-6 T* GPS chip (from *Ublox*) and a *SL1206* antenna (from *Sarantel*) allowing differential positioning and measurement dating. The positioning of the Geocube is possible thanks to raw carrier phase data provided by the *LEA-6 T* chip. This GPS module allows dating the observations of other sensors in the GPS time scale.
- A radio module (RF board; Fig. 1) based on the Xb*ee pro* device (from Di*gi*) to communicate among the Geocube nodes. The frequency used is 2.4 GHz. The main advantage of this radio module is its low energy consumption and the mesh mode used (e.g., every Geocube can route data) through the proprietary protocol *Digimesh*.
- A management module (Microcontroler board; Fig. 1) based on the MSP*430F5438A* micro-controller (from *Texas Instruments*) used for data and sensor management. A 2 GB micro-SD card is used for data recording.

In addition to these three core modules, environmental sensors can be connected either directly to the Geocube if the sensor is small enough, or outside the Geocube if it is large and/or needs a contact with its environment (Fig. 2). For example meteorological sensors, soil humidity probes, pore fluid pressure sensors and seismometers have been successfully coupled to the core modules.

In order to control all the components, a dedicated Operating System (OS) named G3OS is used. It is designed for wireless multi-sensor and remotely-controlled receivers. The OS can operate many simultaneous events ordered by priority even if a single processor is used, and it is also designed to synchronize the *MSP430F5438A* clock on the GPS time scale. Thus, the observations from all sensors of all receivers of a network are recorded in the same time scale. Moreover *G3OS* allows recording data on the micro-SD card in FAT file format, which makes it readable by any computer. Finally *G3OS* can be remotely improved. For this aim, a new release previously tested in the office is send by radio to the Geocube. A simple reset of the device allows then the installation of the new OS release.

2.2. Network deployment and operation mode

Each Geocube is designed to be used as a sensing node of a network. The whole system is composed of several Geocube nodes acting as sensors, a computer coordinator in the field acting as a link between the network and the clients, and one or several client applications running on distant or local computers.

The coordinator is a small Personal Computer (FitPC from *Compulab*). It is equipped by a radio bridge to communicate with the Geocube nodes and by a wired or satellite-based Internet link to communicate with distant computers.

On the coordinator, a daemon (named *serverG3*) is used to manage interactions between the Geocube network and the clients. Each client corresponds to a software dedicated to a specific task (e.g., node positioning, data visualization, and network setting). The clients can be assessed on distant computers connected to Internet or on the coordinator. The user interacts with these softwares using dedicated interfaces (graphical or command line versions). Five types of clients are available (Fig. 3):

- A Graphical User Interface client (GUI) allowing a user to interact with one or several Geocube nodes. It is then possible to

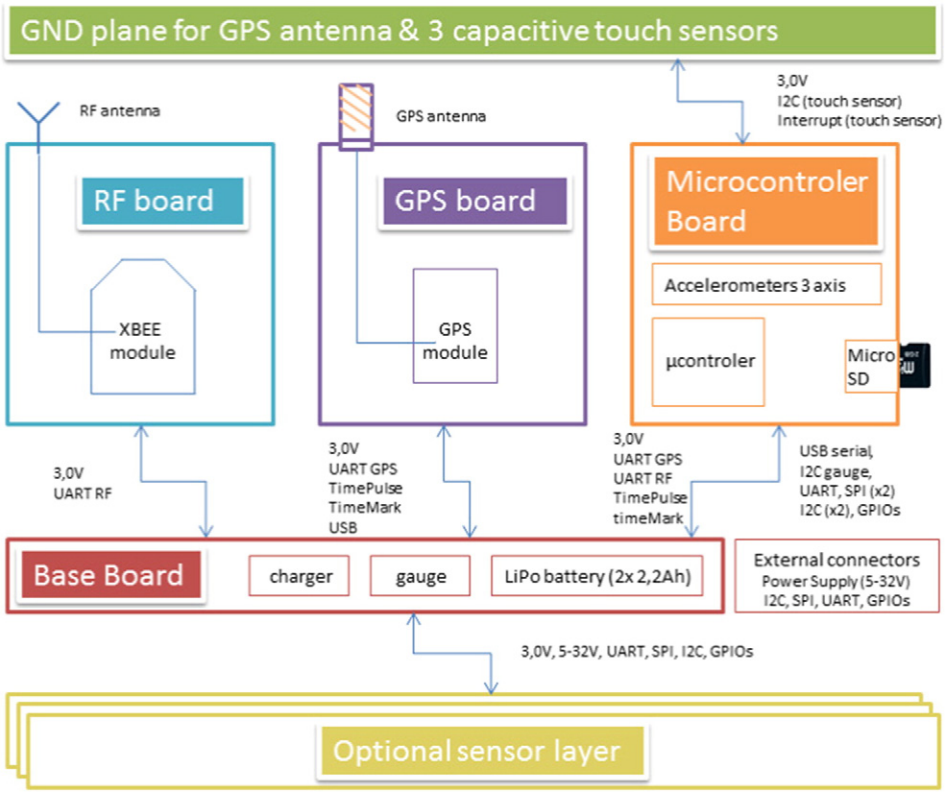

Fig. 1. Hardware architecture of the Geocube system.

communicate with the receiver and to download the observation files;
- A database client used to record and collect the observations;
- A scheduling client sending commands to the Geocube nodes at a given time;
- A downloading client allowing to schedule the download of observation files at a given time;
- A real-time processing client allowing precise positioning from a continuous flow of raw-carrier phase observations.

To reduce the complexity of the daemon *serverG3*, the number of individual clients interacting with one coordinator is limited to seven.

2.3. Calculation of the GPS position

A processing software has been developed for calculating the position of the Geocube receivers from raw carrier phase data (Fig. 4) recorded by the GPS chip. It is optimized for small (a few square kilometers) networks, single-frequency observations and epoch-by-epoch processing (the position time series are computed at the carrier phase acquisition sampling rate). To allow measurements of deformation with a centimeter level accuracy, the algorithm uses relative positioning (i.e., the positions of the moving nodes are known relatively to one or a set of stable nodes). Therefore, carrier phase observations from a series of stable nodes with known coordinates must be included into the network calculation.

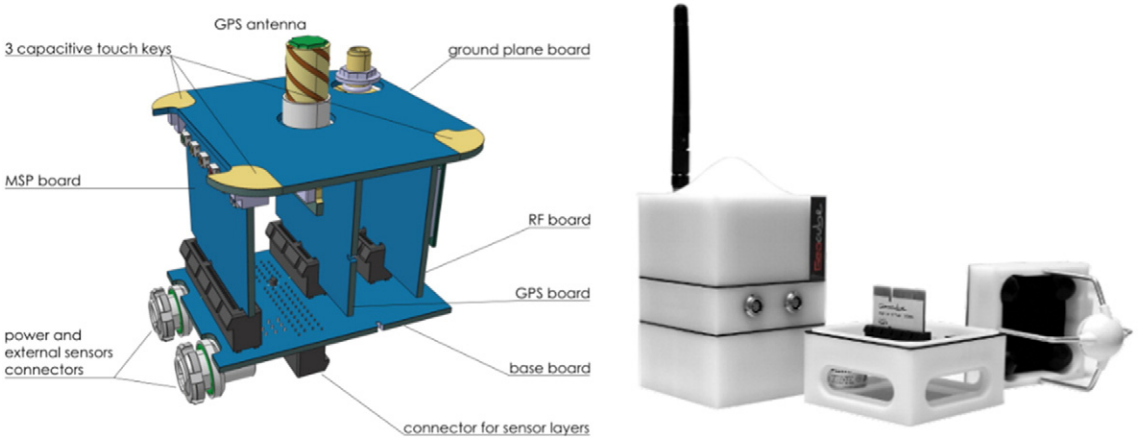

Fig. 2. Instrumental design of a Geocube node. Left: Internal view of a Geocube node. Right: A Geocube node and example of additional sensor layers (from left to right: a Geocube with a radioactivity sensor, an air quality sensor, and a wind speed sensor).

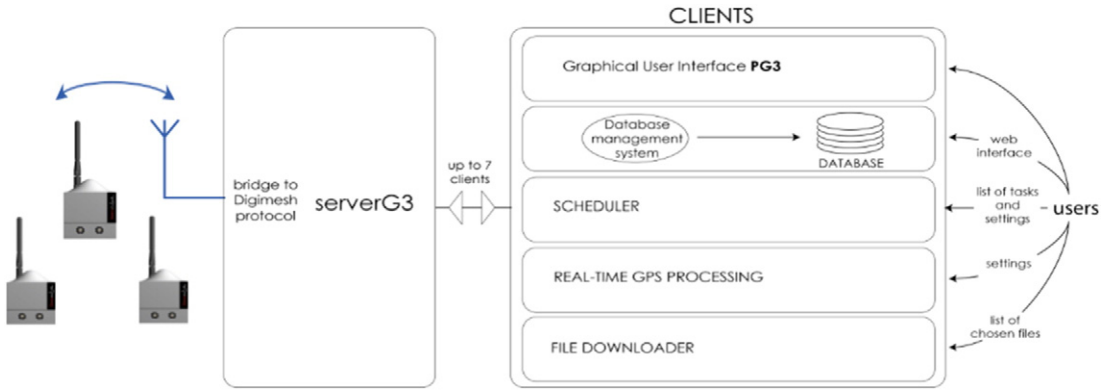

Fig. 3. Framework of a Geocube network and of its clients.

The main features of the processing software (Fig. 4) are presented below focusing on relevant information for the targeted application of landslide monitoring. More details on the processing theory and implementation of the solution are described in Benoit et al. (2014).

The position of the receivers are computed (and updated in the database) each time the GPS observations are sent from the Geocube nodes to the coordinator. To this end, Geocube nodes are programmed to record observations at the same point in time (called epoch) across the whole network using a predefined sampling rate (typically 1 s to 30 s, depending on the application). The observations are sent by radio and are centralized in the coordinator. The data time transfer amounts to 1 to 20 s depending on the size of the network. Then, the relative position of the receivers is calculated from the raw carrier phase observations. The relation (expressed in wave cycles) linking phase observations Φ_r^s with the receiver coordinates X_r, Y_r, Z_r is the carrier phase equation commonly used for precise GPS positioning applied here on the L1 data (Eq. (1))

$$\begin{aligned}\phi_r^s &= \frac{1}{\lambda_{L1}}\cdot\rho_r^s + \frac{c}{\lambda_{L1}}\cdot(dt_r + dt^s) - N_r^s + \tau_{r,iono}^s + \tau_{r,tropo}^s + \varepsilon \\ \rho_r^s &= \sqrt{(X_r - X^s)^2 + (Y_r - Y^s)^2 + (Z_r - Z^s)^2}\end{aligned} \tag{1}$$

where ρ_r^s is the geometric range between the receiver r and the satellite s, X^s, Y^s, Z^s are the coordinates of the satellite s, dt_r and dt^s are respectively the satellite and receiver clock biases; c is the speed of the light in the vacuum; N_r^s is an integer number of wavelength λ_{L1}, $\Delta\tau_r^s{}_{tropo}$ and $\Delta\tau_r^s{}_{iono}$ are the errors due to the wave propagation in respectively the troposphere and ionosphere, and ε is the residual error. In order to remove the major parts of error and bias in Eq. (1), the double

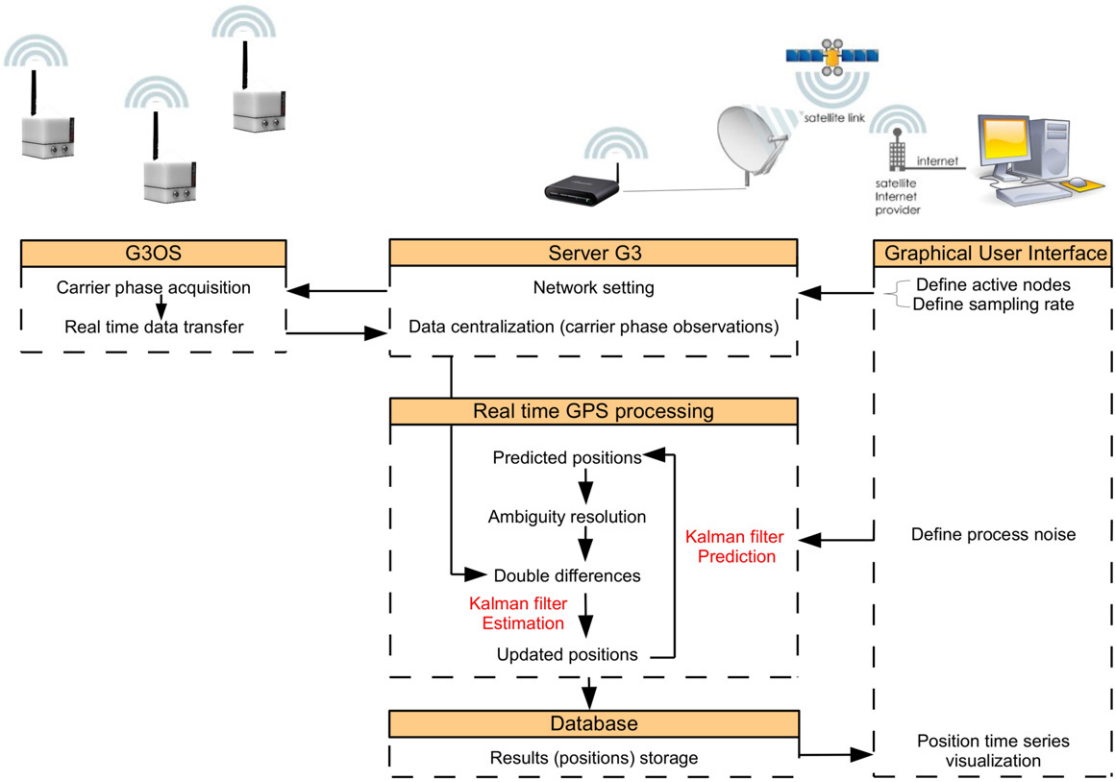

Fig. 4. Acquisition and real-time processing of the GPS observations.

differences combination of carrier phase observation equations is applied between pairs of receivers and satellites (Eq. (2)).

In case of short baselines (typical of local GPS network of less than 5 km), the use of double differences processing discards the clock biases, mitigates the spatially correlated errors and thereby makes the use of L2 data unnecessary for the ionospheric correction (Malet et al., 2002). The actual observation equations used for the calculation of node positions are thus double differences, beforehand corrected using the Saastamoinen model (Saastamoinen, 1972) in order to correct the potential remaining tropospheric effect due to the height difference between the receivers (Eq. (2)). Due to the coarseness of this model, the height difference between the nodes involved in the network must be less than 300 m to ensure a relevant estimate of the position.

$$\nabla\Delta\phi_{r1,r2}^{s1,s2} - \nabla\Delta\tau_{r1,r2,tropo,saastamoinen}^{s1,s2} = \frac{1}{\lambda_{L1}} \cdot \rho_{r1,r2}^{s1,s2} - N_{r1,r2}^{s1,s2} + \varepsilon. \quad (2)$$

An extended Kalman filter is used to compute the receiver positions from double differences for an epoch-by-epoch processing using Eq. (2) as observation equation. The only estimated parameters are the receiver coordinates. Since a network processing is used, the double differences are formed between one master node (arbitrary selected, often the nearest of the coordinator) and all the other Geocube nodes. The carrier phase observations of the master node (r1 in Eq. (2)) thus appears in all double differences used for the positioning, and thereby ensure the link between the observations of the whole network. The observation equations are inverted together over the Kalman filter estimation step (Fig. 4). During the real-time monitoring, the resulting coordinates are available a few seconds after the centralization of raw carrier phase data in the coordinator, approximately 30 s after the carrier phase acquisition by Geocube nodes. In our processing, the ambiguities are solved preliminary using approximate relative position of the Geocube nodes. Such positions are computed from the convergence of a Kalman filtering using triple differences as observations (Remondi and Brown, 2000). This processing is carried out at the installation day of the nodes in the field. It requires around 1 h during which precise positioning is not available. Once the approximate node positions are known, the real-time positioning algorithm can be applied leading to a continuous monitoring.

The main tunable parameter in the Kalman filter is the process noise, which is assumed constant all along the session. It determines the range of position variation allowed to the Geocube nodes during the prediction step (Fig. 4). The process noise is set accordingly with prior assumptions on the nature of the expected movement, and it determines the smoothing of the resulting position time series. If a high process noise ($\sigma_w = 2.10^{-4} \cdot \sqrt{dt}$ m, with dt corresponding to the sampling rate in seconds) is set, each position is estimated almost independently of the previous one. It allows detecting fast displacements, but the resulting position time series are noisy. This noise is mainly due to multipath effects, i.e., local diffusion/reflection of the GPS waves generated by the surrounding antenna environment (Larson et al., 2010). They affect especially the data collected by the Geocube node because the GPS antenna is standard with a lobe geometry that does not reject the major part of the multipaths.

Multipaths are featured by a 10 s to 600 s period (Choi et al., 2004). If only smooth movements are expected in the monitored area, multipaths and displacements have separate frequency spectra. Thus, a low process noise setting in the Kalman filter ($\sigma_w = 2.10^{-6} \cdot \sqrt{dt}$ m) is used to mitigate multipath effects by imposing small displacements between consecutive position estimates; this approach allows to discriminate (smooth) displacements in position estimates and multipaths in residuals. However, displacements and multipaths have rarely totally separated frequency spectra. A compromise between multipath rejection and displacement detection is thus required. The positioning accuracy depends on the magnitude of the expected displacements; the larger displacements are the less accurate due to the incompatibility of strong smoothing and large displacement recording.

The precision and accuracy of the estimated coordinates were assessed during various tests, respectively by computing the a posteriori standard deviations of stable baselines observed under field conditions, and from the analysis of varying baseline lengths during controlled displacement experiments (Benoit et al., 2014). Two to 5 mm in the horizontal component, and 4 to 10 mm in the vertical component a posteriori standard deviations were obtained depending on the process noise used (the best precision is obtained with a low process noise). Note that in the case of a low process noise, up to 6 h of observations are needed for fitting sudden displacements.

According to the instrumental specifications and the processing of the GPS observations, the range of applicability of a Geocube network for landslide monitoring is the following:

- short baselines (<5 km),
- height differences (<300 m),
- surface displacement rates in the range 0.005 m·day^{-1} to 5 m·day^{-1},
- and installation of the nodes on stable and rigid structures to ensure a coupling of the receivers with the deforming media.

3. Field application: monitoring of the Super-Sauze landslide with a dense Geocube network

3.1. Geomorphological setting of the Super-Sauze landslide

The Super-Sauze landslide is representative of mass movements developed in clay-shale deposits. It is located in the Barcelonnette Basin in the Southeast French Alps (Fig. 5) and has been triggered in the 1960s. The landslide has a length of 950 m from the main scarp to the toe, and is up to 150 m in width. The difference in elevation is around 300 m. The topographic surface displays several deformation features such as ridges, bulges, lobes and fissures but also surface erosion features such as rills and small gullies. The landslide features highly variable displacement rates (from 0.005 m·day^{-1} to 0.03 m·day^{-1}). The displacement field is heterogeneous in time and space (Fig. 5) because of local interactions between the moving mass and the stable bedrock (Travelletti and Malet, 2012; Travelletti et al., 2012). The general direction of the displacements is facing N-10° in the upper part and N-340° in the lower part in relation to the bedrock geometry. In general, a decrease in the displacement rates is observed from the top to the bottom of the landslide indicating an accumulation of material in the lower part (Travelletti and Malet, 2012).

During the last 20 years, the landslide has been investigated through numerous monitoring campaigns including GPS surveys (Malet et al., 2002), in-situ hydro-geophysical measurements (Malet et al., 2005), repeated terrestrial and airborne LiDAR (Light-Detection and Ranging) observations (Travelletti et al., 2014), and the acquisition of aerial or terrestrial optical imagery (Travelletti et al., 2012; Niethammer et al., 2012). Several years (1996–2014) of continuous displacements and pore water pressure monitoring have demonstrated that the slope accelerations are controlled by hydro-climatic factors (rain, snow melt) (Bernardie et al., 2014) and are generally the result of the undrained reactivation of the reworked material (Malet et al., 2005). The kinematic regime has a marked seasonal trend with two acceleration periods in spring and autumn (Fig. 5), and two deceleration periods, in winter (when snow covers the landslide) and in summer.

3.2. The Geocube monitoring network of Summer 2012

A monitoring campaign with a network of nineteen Geocube nodes was carried out during 82 days in summer 2012 (from 2012/07/06 to 2012/09/26). Sixteen Geocube nodes were installed in the upper part

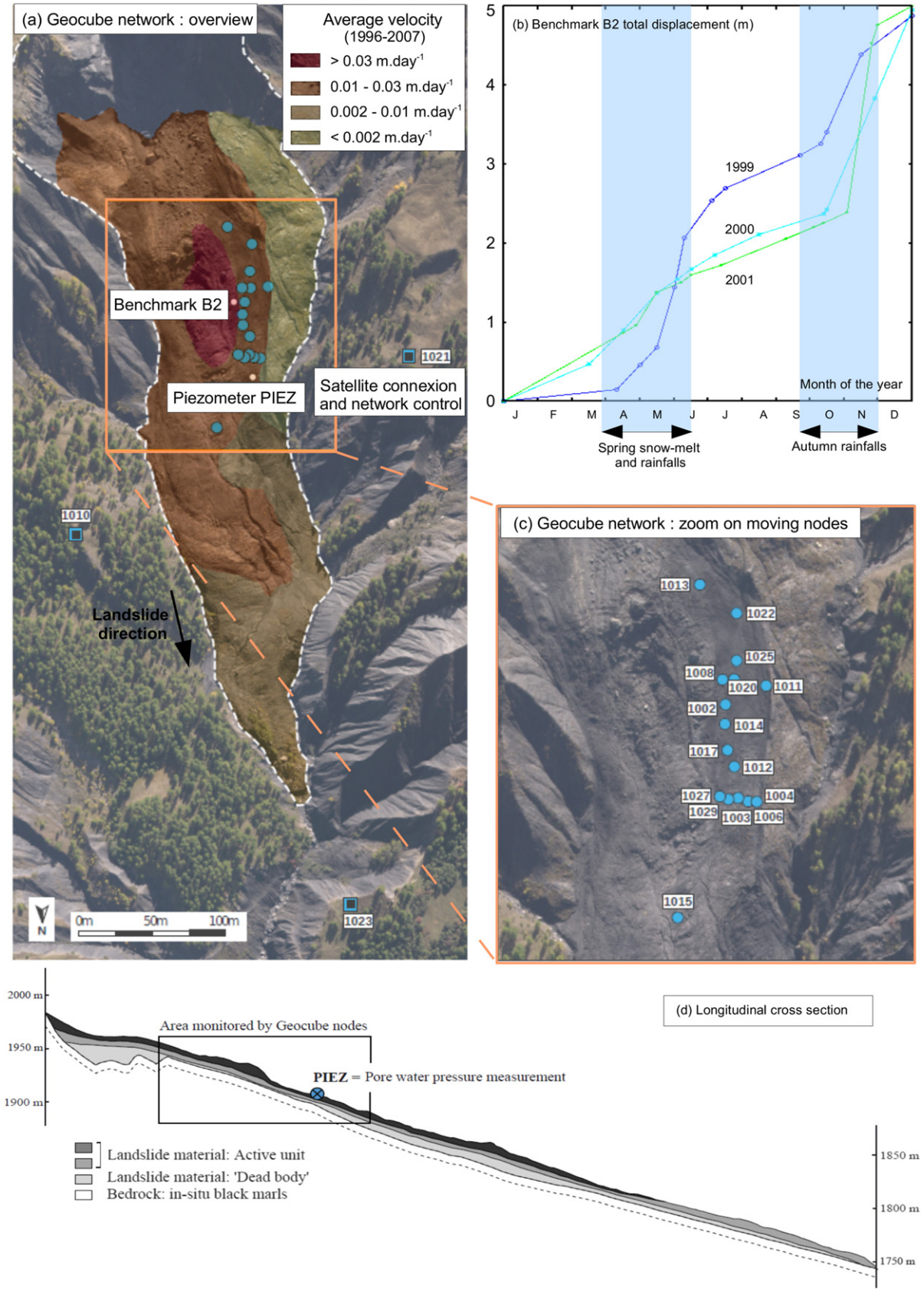

Fig. 5. Study area. (a) and (c): Location of the Geocube nodes installed for the monitoring campaign; the Geocube network has been installed in the upper part of the landslide where the displacement rates are the highest. (a), (b) and (c): Previous knowledge on the landslide and the displacement field, adapted from (Bernardie et al., 2014; Travelletti and Malet, 2012). The longitudinal cross-section (c) highlights the spatial distribution of the displacement in relation to the shape of the stable bedrock, the depth of the landslide material and the slope angle of the surface topograph.

of the landslide in an area with large displacement rates (Amitrano et al., 2007; Bernardie et al., 2014), and three Geocubes nodes were installed on stable slopes surrounding the landslide (Fig. 5). The nodes were fixed on PVC tubes filled with concrete and anchored in the topsoil over a length of 30 cm (Fig. 6). The distance between the Geocube nodes installed on the landslide was around 20 m to allow measuring the displacement field at a high spatial resolution (Fig. 5). The coordinator node and a satellite antenna for Internet connection were located close to the Geocube receiver 1021 on the Western slope of the landslide in order to overlook the whole network and facilitate the radio link.

In addition to the GPS observations, meteorological and hydrological sensors were installed and connected to the Geocubes. These sensors consisted in air pressure, air temperature and air humidity measurements (at Geocube receiver 1015), rainfall, wind velocity and wind direction (at Geocube receiver 1021), soil temperature and soil water content (at Geocube receivers 1006, 1008 and 1020) and soil water tension set up around 60 cm underground (at Geocube receivers 1006 and 1020). Some of these Geocube nodes with their environmental sensors are presented in Fig. 6. Groundwater level observations monitored in a piezometer operated by OMIV (PIEZ, Fig. 5) are also used.

The instrumental status of the receivers (power consumption and management, data storage and data transmission), the quality of the GPS positioning and the quality of the environmental sensors added to the GPS receivers were tested. In terms of positioning, the test site is challenging because a crest to the South creates a 40° topographic mask reducing the skyview of the GPS satellite constellation.

3.3. Performance of the Geocube hardware

Due to experimental conditions, 62% of the potential observations were acquired. Fig. 7 summarizes the completeness of the observations for all receivers and itemizes the causes of malfunctioning. Observation loss corresponding to a lack of power supply was caused by technical problems with four solar panels at the beginning of the survey period. They were then replaced and after this maintenance, the affected receivers worked well. The environmental sensors acquired data when the corresponding Geocube nodes operated well, but receivers 1006, 1008 and 1020 present a loss of observations due to a lack of sealing induced by the connection of external soil temperature and humidity sensors. The meteorological sensors of receivers 1021 and 1015 did not disturb the GPS acquisition and all the observations are available.

The network aspect was also tested during this experiment. Working receivers could be queried by users along the whole monitoring campaign. The download of observation files stored locally in SD memory cards was successfully carried out, as well as experiments of real-time radio data transfer for real-time positioning.

However, we experienced some troubles for coordinator power supply due to mis-sized solar panels and batteries regarding the high power consumption of the master station (mainly due to the satellite Internet connexion used). This forced us to shut down this coordinator node during the nights, thereby avoiding a continuous real-time monitoring of the landslide. Yet a better power supply facility should fix this problem. In order to test the Geocube positioning performances despite this limitation, the raw data were stored in situ in the SD card of the Geocube nodes during the whole session, and post-processed off line at the end of the session.

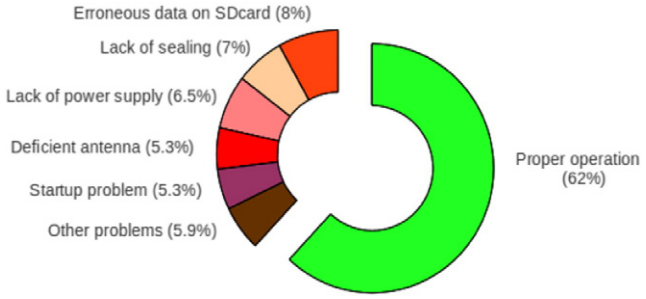

Fig. 7. Instrumental status of operation of the Geocube nodes during the monitoring campaign of 82 days.

3.4. GPS data processing

GPS raw carrier phase were acquired at a 30 s sampling rate and stored on SD memory cards. At the end of the session, the data are downloaded on a computer and processed by the positioning algorithm presented in Section 2.3 implemented in a post-processing module. This module mimics the real-time processing, the only difference being that it uses the raw carrier phase data stored in files in spite of carrier phase data sent by radio. For the processing, a 10° cut-off angle and epochs with three or more satellite phase data were used. In order to constrain the solution during poor GPS constellation periods, a process noise of $\sigma_w = 2.10^{-6} \cdot \sqrt{dt}$ m was setup in the Kalman filter. This filter allows rejecting a part of the multipaths on residuals without a miscalculation of the positions because of the smooth nature of the displacements. As an example, a 40-day session (from 2012/08/01 to 2012/09/09) of observation, selected for the trade-off between the number of working nodes and the session length, is presented in Figs. 8 and 9. During this session, nine Geocube nodes were acquiring observations without any loss, and five additional nodes worked discontinuously. Two stable Geocube nodes (1021, 1010) set up on stable slopes surrounding the landslide were used as references.

In order to ensure the stability of the references and to assess the real precision of the processing for site-specific acquisition conditions, the baseline between the fixed receivers is processed (Fig. 8).

For this baseline, the three components show long-term stability with daily oscillations due to remaining multipath effects and the 23 h and 56 min repeat time of the GPS constellation (Agnew and Larson,

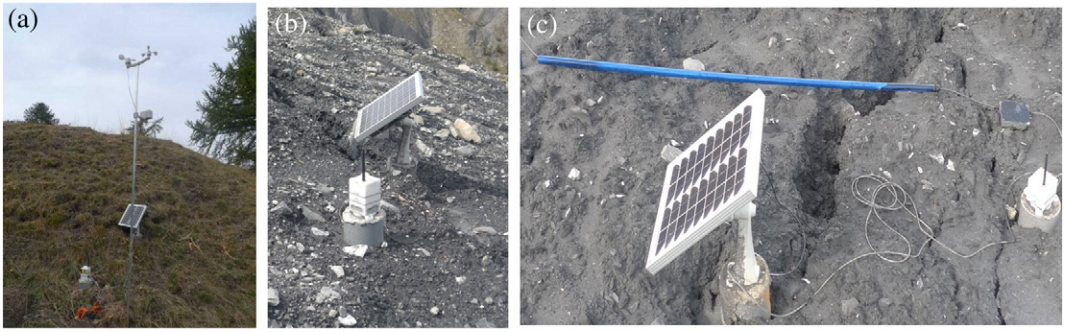

Fig. 6. Installation of the Geocube nodes in the field. (a) Geocube receiver 1021 installed on a stable slope surrounding the landslide with a wind sensor and a rain gauge . (b) Geocube receiver 1015 with air temperature and air humidity sensors. (c) Geocube receiver 1008 with ground temperature and soil water content sensors.

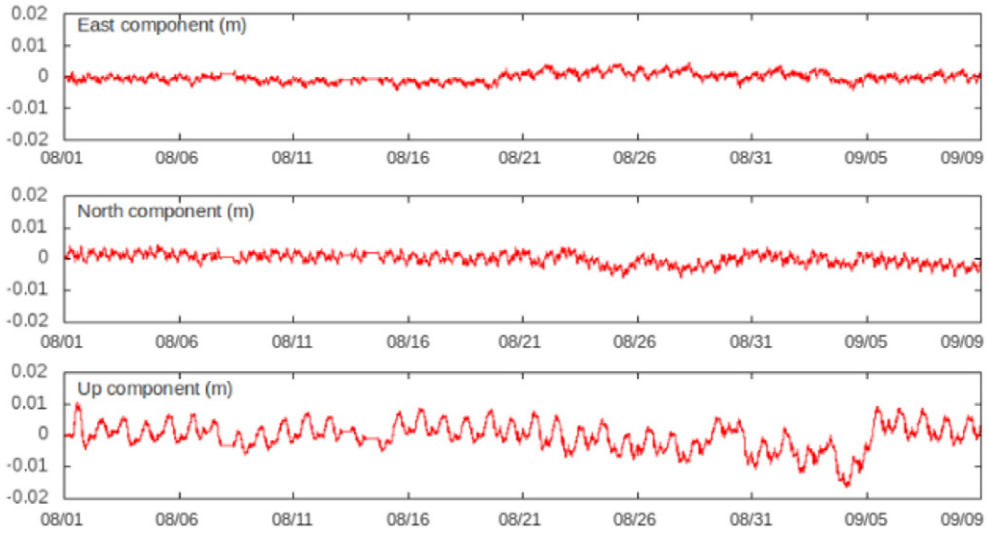

Fig. 8. Time series of the baseline (three components, 30 s sampling rate) between the Geocube receivers 1021 and 1010 installed on stable slopes. The period of measurements extents from 2012/08/01 to 2012/09/09.

2007). The Up component has a three time larger dispersion than the horizontal components which is characteristic of GPS positioning because all visible satellites are located on a half-sphere above the receivers. Some larger variations in the daily coordinates occur at 08/20 - 08/23, 08/30 and 09/03 - 09/05 which are rainy days. During these rainy days, the amplitude of the multipath changes (Larson et al., 2010) inducing a temporary bias on the estimated positions. For the 40-day session, displacement records present a standard deviation of respectively 2 mm and 5 mm for the horizontal and vertical components. The repeatability of the displacements is similar to the one obtained in the same conditions by geodetic grade GPS receivers (Malet et al., 2002) and confirms the relevance of the adopted positioning strategy based on a local network of single frequency low-cost GPS receivers.

3.5. Analysis of displacement pattern

The data collected by the Geocubes allowed estimating continuous, high frequency 3D positions for many sensing points (Fig. 9). Hereafter only the results of the horizontal component, less noisy, are presented and discussed. A mesh of horizontal displacement rates (Fig. 9a) is obtained for a 10-day period (2012/08/05–2012/08/14) in which 14 Geocubes nodes acquired data. The measured displacement rates

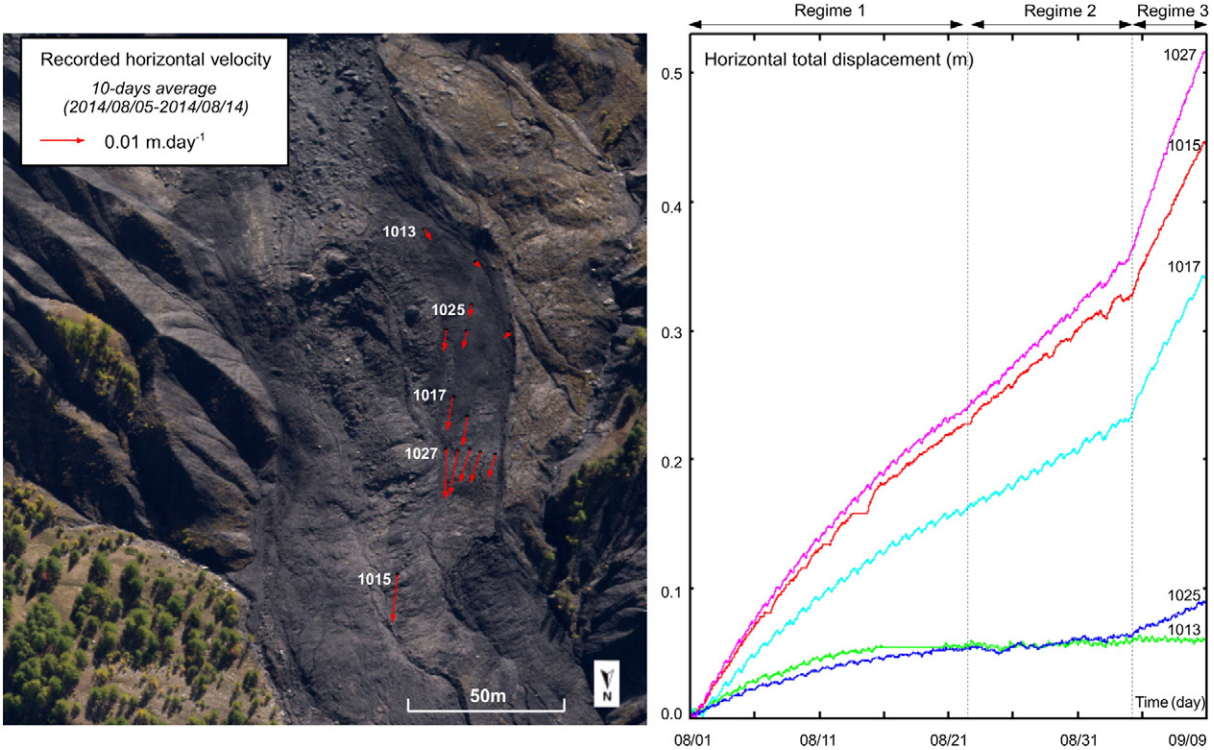

Fig. 9. Kinematics of the landslide during the monitoring period. Left: Measured horizontal mean velocity (2012/08/05 – 2012/08/14); Right: Horizontal cumulative displacements (2012/08/01–2012/09/09).

show a large spatial heterogeneity. Gradients of displacement rates are observed in the north–south and east–west directions. The displacement rates increase from less than 0.0025 m·day^{-1} at the top of the landslide to up to 0.01 m·day^{-1} downslope of the monitoring area. Higher displacement rates are recorded in the central part of the landslide than on the lateral sides. The displacement field (Fig. 9a) is in agreement with previous knowledge (Amitrano et al., 2007, summarized by Fig. 5), indicating that a lateral gradient of displacement rates and velocities close to 0.01 m·day^{-1} were measured.

Time series of horizontal cumulative displacements at a 30 s time resolution are also computed for the Geocube nodes working during the 40-day session. Fig. 9b shows the results for five nodes distributed along the landslide and spaced from 20 m to 50 m. Three different flow regimes can be identified: 08/01–08/20, 08/21–09/04 and 09/04–09/09 (Figs. 9b, 10).

The number and spatial distribution of the sensing nodes allow computing the strain tensors from the recorded displacements (Fig. 10). Unfortunately, due to the network configuration, the spatial resolution remains coarse in view of continuum mechanics. However, the strain tensors give important information about the deformations of the landslide. The tensors are calculated for three periods corresponding to the kinematic regimes identified above: 08/08–08/14 (regime 1), 08/21–08/30 (regime 2), 08/31–09/09 (regime 3). As the number of nodes is limited, a Delaunay triangulation between Geocubes nodes was adopted as background mesh. At each node of the mesh having coordinates (x,y), Eq. (3) gives the relation between the elementary deformation $\left(\frac{\partial u}{\partial x}, \frac{\partial u}{\partial y}, \frac{\partial v}{\partial x}, \frac{\partial v}{\partial y}\right)$ for the main directions of a local coordinate system (O,X,Y) and the strain tensor ε.

$$\varepsilon = \begin{pmatrix} \dfrac{\partial u}{\partial x} & \dfrac{1}{2}\left(\dfrac{\partial u}{\partial y} + \dfrac{\partial v}{\partial x}\right) \\ \dfrac{1}{2}\left(\dfrac{\partial u}{\partial y} + \dfrac{\partial u}{\partial x}\right) & \dfrac{\partial v}{\partial y} \end{pmatrix}. \tag{3}$$

As ε is a real and symmetric matrix, it can be diagonalized. The eigenvectors give the direction of the principal strains and the eigenvalues give the amplitude. A positive eigenvalue indicates extension while a negative eigenvalue indicates compression. The diagonalized strain tensor provides an image of the strains experienced by the elementary triangle used for the calculation (Fig. 10).

4. Discussion: analysis of the landslide displacement pattern

During the field campaign, 40 days of GPS observations are available, during which some rainy events occurred between 2012/08/19 and 2012/09/05. This relatively restricted amount of observations is justified by the initial purpose of the experiment which aimed at testing the performance of the Geocube nodes in field conditions. Moreover, due to the low number of available meteorological and soil water content sensors connected to the Geocubes and their failure rate, the factors conditioning the landslide behavior were not recorded at a high spatial density.

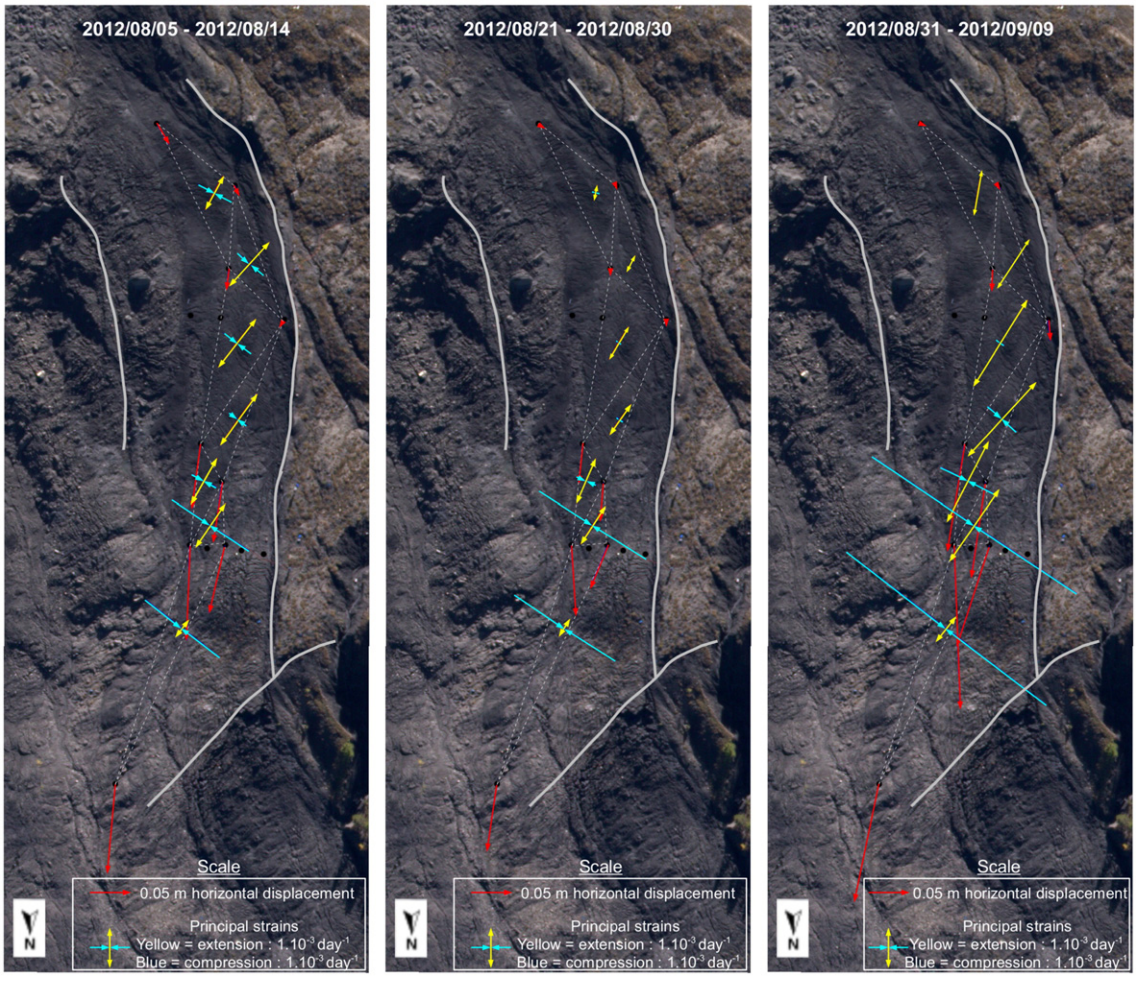

Fig. 10. Strains estimated at the Super-Sauze landslide (2012/08/05–2012/09/09). The red arrows depict the horizontal displacements; the yellow and blue arrows indicate the principal strain directions. Compression is highlighted in blue, extension is highlighted in yellow. The triangulation used for the strain tensor calculation is indicated in dashed white. The gray lines denote the location of the buried crests of the bedrock channelizing the landslide material.

Despite these limitations, the results of the experiment give new insights on the Super-Sauze landslide behavior, and allow to document a transient acceleration in a period of low ground water table level.

Fig. 10 presents the horizontal displacements and strains generated by the landslide movement and the interaction with the bedrock geometry (Travelletti and Malet, 2012). In the monitored area, the landslide motion is channelized by two buried crests. The curvature of the channel at the top of the area induces compression of the sliding material due to the presence of the Western crest. Downslope, the motion is orientated along the north–south direction (e.g., parallel to the buried crests). At the lower part of the monitoring area, the motion decelerates because of the presence of a buried crest nearly perpendicular to the sliding direction (Gance et al., 2012) and compression is generated (Geocubes nodes 1003 and 1015). This compression at the bottom increases with the displacement rate during the period in regime 3 (08/31–09/09). Simultaneously, as the motion decelerates at the top, extension increases in the middle part of the area generating cracking at the surface (Stumpf et al., 2013). These tension cracks are easily visible on the background orthophotograph of Fig. 10. The direction of the cracks is orthogonal to the extension axis of the strain tensors. Such behavior is consistent with the theory of plastic failure as sliding and yielding lead to rapid accumulation of plastic strains and sometimes to large failure (Araiba and Suemine, 2007; Pudasaini, 2012). Further, dilatancy of the material (e.g., succession of compression and extension sequences in space and time according to pore pressure feedbacks) is monitored by the Geocube nodes, allowing to document the complex hydro-mechanical coupling controlling the landslide dynamics (Iverson et al., 2000; Iverson, 2005).

Displacement and strain rates show temporal variations (Figs. 9; 11). In order to investigate the three flow regimes identified above (Fig. 9), daily averaged displacement rates are calculated (Fig. 11) and compared with the rainfall amount measured at Geocube node 1021 and to the groundwater table variations at piezometer PIEZ (Fig. 5). Focusing on the five Geocube nodes distributed along the landslide, the three sliding regimes are confirmed: first a period with a progressive lowering of displacement rates for all nodes occurs until the day 08/20, then the displacement rate is constant from day 08/21 to day 09/04, and finally a period of increasing displacement rates starts on 09/04 (Fig. 10).

The first regime corresponds to the end of a long dry period (58 days without any rain) during which the drop of displacement rate is explained by the drainage of the groundwater table.

The second regime corresponds to the start of a low amplitude reactivation of the sliding for the Geocubes nodes 1027, 1015 and 1017, while the Geocubes nodes 1013 and 1015 are still in a stationary phase taking into account the measurement precision. The reactivation is triggered by a moderate rainfall (25 mm in 4 days, from 08/20 to 08/23) not sufficient to rise the groundwater table level at the location of the piezometer PIEZ. After this transient phenomenon, a groundwater table increase is observed at day 08/25. The pore water pressure rise stops the drop of displacement rates, but is not large enough to accelerate the sliding. The time lag between the sliding reactivation (08/22) and the groundwater table rise (08/25) can be explained by the complex hydrology of the landslide with different response of the slope to rainfall according to the initial soil water content nearby the piezometer PIEZ. A denser network of groundwater table measurements would be necessary to understand such transient acceleration for instance by adding piezometers at all Geocube nodes.

The third regime corresponds to an important acceleration of the landslide triggered by a sequence of heavy rainfalls (55 mm in 3 days) and a ground water table level rise (20 cm) from day 09/03 to day 09/05. Such acceleration follows the pattern of sliding reactivation observed at Super-Sauze landslide since the start of the long-term monitoring (Malet et al., 2002, 2005). The tiny difference of ground water table levels between this regime of acceleration and the previous very limited reactivation suggests that the pore water pressure threshold

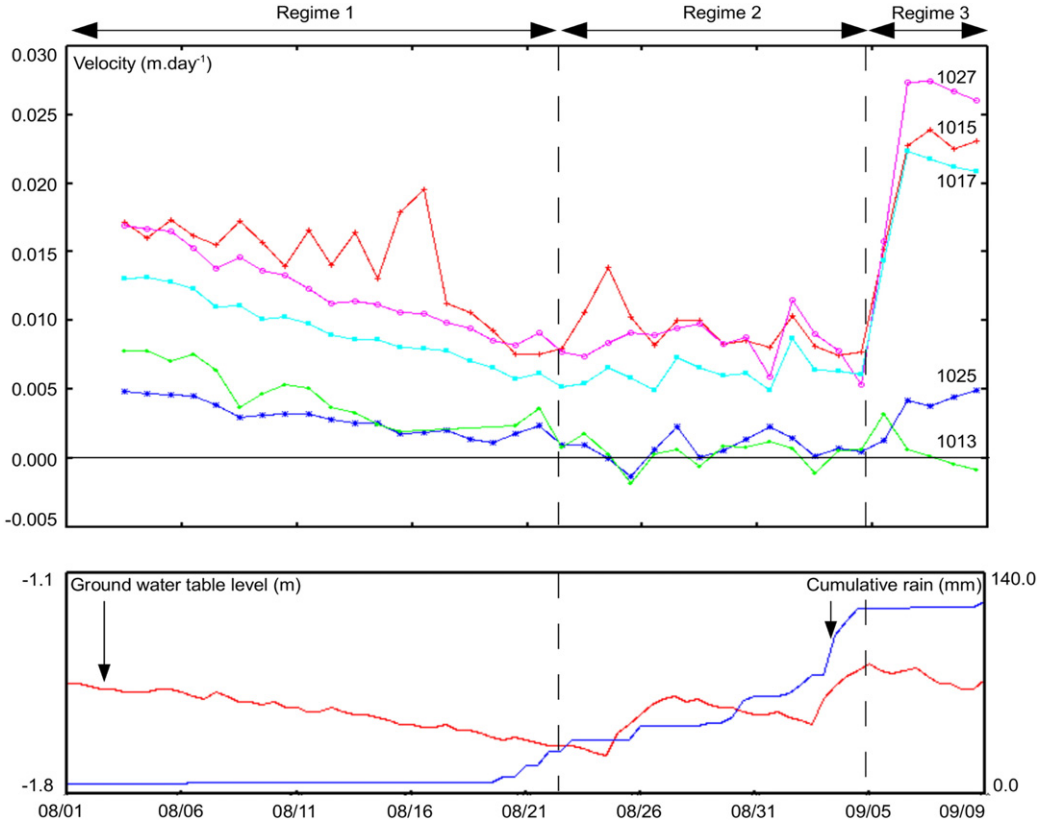

Fig. 11. Motion of the Super-Sauze landslide during a period of low ground water table (2012/08/01–2012/09/09). Top: Daily average horizontal displacement rates for five Geocube nodes. Bottom: Cumulative rain measured at Geocube node 1021 and ground water table level measured at piezometer PIEZ.

controlling acceleration was only weakly exceeded. The acceleration is large for the faster nodes (up to +300% increase in displacement rates) but its amplitude decreases upslope; the movement of the nodes located at the top of the monitoring area (Geocube 1013) is not increasing. The acceleration pattern of Geocube node 1025 is interesting because this acceleration is more progressive than the other nodes. This can be explained by the position of this node at the upper boundary of an area moistened by a spring located near Geocube node 1025 and visible in the field after heavy rainfall or during periods of snow-melt in spring (Travelletti, 2012). This local water input in addition to rainfall can explain the sliding reactivation downhill of Geocube node 1025 but not upslope.

5. Conclusion

The Geocube system allows monitoring landslide behavior at high spatial density, high time resolution and with multiple sensors. Several technical and instrumental characteristics of the Geocube system are particularly interesting for landslide monitoring.

First, the receivers can be deployed relatively quickly where a precise deformation measurement is needed. This flexibility is possible thanks to the low cost of the receivers and their easy deployment (wireless system, low power consumption supplied by small solar panels). The dense spatial sampling of the deformation allows recording the spatial heterogeneity of the displacement field and obtaining advanced information such as variations in strain rates.

Second, the temporal frequency (30 s positioning sampling rate) allows recording dynamic and transient responses of the slope to the forcing. The high time resolution observations are only useful if the accuracy of the positioning is high. With the Geocube system, the high accuracy is obtained because of the short baselines between the receivers. Thus Geocube dense networks are limited to the monitoring of small areas (baselines < 5 km). For such networks, a sub-centimeter level accuracy is reached even under difficult field conditions and for an epoch-by-epoch processing.

The performances of the Geocube system were successfully tested during a field experiment at the Super-Sauze landslide. The displacement measurements were used to investigate an end-of-summer sliding reactivation. The spatial heterogeneity of the acceleration are highlighted for the first time. Although the results show the potential of the Geocubes, further data acquisitions are requested to fully investigate the landslide dynamics. The setting up of a permanent Geocube network at the Super-Sauze landslide is currently considered.

Acknowledgments

The piezometer observations are provided by the French Landslide Observatory (OMIV: Observatoire Multidisciplinaire des Instabilités de Versants: http://omiv.unistra.fr).

References

Agnew, D., Larson, K., 2007. Finding the repeat times of the GPS constellation. GPS Solutions 11, 71–77.
Amitrano, D., Gaffet, S., Malet, J.-P., Maquaire, O., 2007. An experience of seismic monitoring for understanding muddy landslides: the case of Super-Sauze (South French Alps). Bull. Soc. Geol. Fr. 178 (2), 149–157.
Araiba, K., Suemine, A., 2007. Enlargement of a failed area along a sliding surface. In: Sassa, K., Fukuoka, H., Wang, F., Wang, G. (Eds.), Progress in Landslide Science. Springer, Heidelberg, pp. 229–236.
Azzam, R., Arnhardt, C., Fernandez-Steeger, T.M., 2010. Monitoring and early warning of slope instabilities and deformations by sensor fusion in self-organized wireless ad-hoc sensor networks. International Symposium and the 2nd AUN/Seed-Net Regional Conference on Geo-Disaster Mitigation in ASEAN — Protecting Life from Geo-Disaster and Environmental Hazards, February 25–26, 2010, Bali, Indonesia, pp. 157–164.
Benoit, L., Briole, P., Martin, O., Thom, C., 2014. Real-time deformation monitoring by a wireless network of low-cost GPS. J. Appl. Geod. 8, 119–128.
Bernardie, S., Desramaut, N., Malet, J.P., Gourlay, M., Grandjean, G., 2014. Prediction of changes in landslide rates induced by rainfall. Landslides, http://dx.doi.org/10.1007/s10346-014-0495-8.
Buchli, B., Sutton, F., Beutel, J., 2012. GPS-equipped wireless sensor network node for high-accuracy positioning applications. In: Picco, G.P., Heinzelman, W. (Eds.), EWSN 2012. LNCS 7158, pp. 179–195.
Cattin, P., Brahier, J., 2011. Géomonitorage par GPS avec des équipements à faible coût. Géomatique Suisse 06/2011, 306–308.
Choi, K., Bilich, A., Larson, K., Axelrad, P., 2004. Modified sidereal filtering: implications for high-rate GPS positioning. Geophys. Res. Lett. 31, http://dx.doi.org/10.1029/2004GL021621.
Gance, J., Grandjean, G., Samyn, K., Malet, J.-P., 2012. Quasi-Newton inversion of seismic first arrivals using source finite bandwidth assumption: application to subsurface characterization of landslides. J. Appl. Geophys. 87, 94–106.
Heunecke, O., Glabsch, J., Schuhbäck, S., 2011. Landslide monitoring using low cost GNSS equipment — experiences from two Alpine testing sites. J. Civ. Eng. Archit. 45, 661–669.
Iverson, R.M., 2005. Regulation of landslide motion by dilatancy and pore pressure feedback. J. Geophys. Res. 110, http://dx.doi.org/10.1029/2004JF000268.
Iverson, R.M., Reid, M.E., Iverson, N.R., LaHusen, R.G., Logan, M., Mann, J.E., Brien, D.L., 2000. Acute sensitivity of landslide rates to initial soil porosity. Science 290, 513–516.
Jaboyedoff, M., Oppikofer, T., Abellan, A., Derron, M.H., Loye, A., Metzger, R., Pedrazzini, A., 2012. Use of LiDAR in landslide investigation/a review. Nat. Hazards 61 (1), 5–28.
Larson, K., Braun, J., Small, E., Zavorotny, V., Gutmann, E., Bilich, A., 2010. GPS multipath and its relation to near-surface soil moisture content. IEEE J. Sel. Topics Appl. Earth Observ. Remote Sens. 3, 91–99.
Malet, J.-P., Hartig, S., Calais, E., Maquaire, O., 2000. Apport du GPS au suivi en continu des mouvements de terrain. Application au glissement-coulée de Super-Sauze. C.R. Acad. Sci., Ser. IIa: Sci. Terre Planets 331, 175–182.
Malet, J.-P., Maquaire, O., Calais, E., 2002. The use of Global Positioning System for the continuous monitoring of landslides. Application to the Super-Sauze earthflow (Alpes-de-Haute-Provence, France). Geomorphology 43, 33–54.
Malet, J.-P., van Asch, Th.W.J., Van Beek, R., Maquaire, O., 2005. Forecasting the behaviour of complex landslides with a spatially distributed hydrological model. Nat. Hazards Earth Syst. Sci. 5, 71–85.
Niethammer, U., James, M., Rothmund, S., Travelletti, J., Joswig, M., 2012. UAV-based remote sensing of the Super-Sauze landslide: evaluation and results. Eng. Geol. 2012 (128), 2–11.
Peters, E.T., Malet, J.-P., Bogaard, T.A., 2010. Multi-sensor monitoring network for real-time landslide forecasts in early warning systems. In: Malet, J.-P., Glade, T., Casagli, N. (Eds.), Proceedings of the International Conference "Mountain Risks: Bringing Science to Society". CERG Editions, Strasbourg, pp. 335–340.
Pudasaini, S.P., 2012. A general two-phase debris flow model. J. Geophys. Res. 117, http://dx.doi.org/10.1029/2011JF002186.
Remondi, B., Brown, G., 2000. Triple differencing with Kalman filtering: making it work. GPS Solutions 3, 58–64.
Squarzoni, C., Delacourt, C., Allemand, P., 2005. Differential single-frequency GPS monitoring of the La Valette landslide (French Alps). Eng. Geol. 79, 215–229.
Stumpf, A., Malet, J.P., Kerle, N., Niethammer, U., Rothmund, S., 2013. Image-based mapping of surface fissures for the investigation of landslide dynamics. Geomorphology 186, 12–27.
Takasu, T., Yasuda, A., 2008. Evaluation of RTK-GPS performance with low-cost single-frequency GPS receivers. International Symposium on GPS/GNSS 2008.
Saastamoinen, J., 1972. Atmospheric correction for the troposphere and stratosphere in radio ranging of satellites. In: Henriksen, S.W., Mancini, A., Chovitz, B.H. (Eds.), The Use of Artificial Satellites for Geodesy. Geophys. Monogr. Ser. vol 15. AGU, Washington, D.C., pp. 247–251.
Travelletti, J., 2012. Imagerie multi-paramètres et multi-résolutions pour l'observation et la caractérisation des mécanismes de glissements-coulées PhD Thesis, Université de Caen-Basse-Normandie (271 pp.).
Travelletti, J., Malet, J.-P., 2012. Characterization of the 3D geometry of flow-like landslides: a methodology based on the integration of heterogeneous multi-source data. Eng. Geol. 128, 30–48.
Travelletti, J., Delacourt, C., Allemand, P., Malet, J.-P., Schmittbuhl, J., Toussaint, R., Bastard, M., 2012. A multi-temporal image correlation method to characterize landslide displacements with a terrestrial camera. Int. J. Appl. Earth Obs. Geoinf. 70, 39–55.
Travelletti, J., Malet, J.-P., Delacourt, C., 2014. Image-based correlation of laser scanning point cloud time series for landslide monitoring. Int. J. Appl. Earth Obs. Geoinf. 32, 1–18.